Journal of Colloid and Interface Science 330 (2009) 359–366

Contents lists available at ScienceDirect

Journal of Colloid and Interface Science

www.elsevier.com/locate/jcis

Synthesis of nickel nanoparticles supported on metal oxides using electroless plating: Controlling the dispersion and size of nickel nanoparticles

Zhijie Wu, Shaohui Ge, Minghui Zhang *, Wei Li, Keyi Tao

Institute of New Catalytic Materials Science, College of Chemistry and Engineering Research, Center of High-Energy Storage & Conversion (Ministry of Education), Nankai University, Tianjin 300071, China

ARTICLE INFO

Article history:
Received 13 August 2008
Accepted 28 October 2008

Keywords:
Electroless plating
Nickel
Nanoparticles
Interface reaction
Metal oxide
Deposition

ABSTRACT

Nickel nanoparticles supported on metal oxides were prepared by a modified electroless nickel-plating method. The process and mechanism of electroless plating were studied by changing the active metal (Ag) loading, acidity, and surface area of metal oxides and were characterized by UV–vis spectroscopy, transmission electron microscopy, scanning electron microscopy, and H_2 chemisorption. The results showed that the dispersion of nickel nanoparticles was dependent on the interface reaction between the metal oxide and the plating solution or the active metal and the plating solution. The Ag loading and acidity of the metal oxide mainly affected the interface reaction to change the dispersion of nickel nanoparticles. The use of ultrasonic waves and microwaves and the change of solvents from water to ethylene glycol in the electroless plating could affect the dispersion and size of nickel nanoparticles.

1. Introduction

Interest in clusters or nanoparticles with properties distinct from those of individual atoms and molecules or bulk matter has been widespread [1]. Supported nickel nanoparticles have been reported frequently in magnetic science and catalysis science. In particular, nickel nanoparticles supported on metal oxides with unique chemical and physical properties have been widely used as catalysts for many hydrorelated reactions, such as the hydrogenation, hydrogenolysis, and hydrotreating reactions [1–6]. Such supported nickel nanoparticles are mostly synthesized by the impregnation/deposition of nickel complexes from an aqueous solution onto the supports [4]. Metal oxide in aqueous suspension is generally electrically charged, as shown in Fig. S1 (the scheme of the adsorption of metal ions by metal oxides in aqueous suspension with different pHs) [2], and an "equilibrium deposition filtration" (EDF) method is widely used for the synthesis of supported nickel nanoparticles [1–3]. The dispersion of nickel nanoparticles is very high, as the nickel loading on supports is low (below 5 wt%, mostly) [4,5]. But the EDF method cannot be applied in such cases when a higher nickel loading (e.g., >15 wt%) or a controllable particle size of nickel nanoparticles is required. Incipient wetness impregnation, wet impregnation, pore volume impregnation, dry impregnation, and nondry impregnation without filtration have been extended to increase the nickel loading and the particle size, although the dispersion of nickel nanoparticles is relatively lower [4]. Indeed, a new method for the synthesis of supported nickel nanoparticles with high dispersion as well as high nickel loading is significant for their further catalytic application. The electroless nickel-plating method should be a suitable choice because it has been proved to control the nickel loading, particle size, and dispersion of nickel nanoparticles [4–6].

The electroless nickel plating should first be activated by active substrates preloaded with Ni, Ag, Au, Pd, or Pt metal. The plating occurs by the reduction of nickel ions at the surface of the active substrate immersed into the plating solution and continues to deposit on the substrate through a catalytic action of the deposit itself [7–9]. Two mechanisms of electroless plating with borohydride as reductant have been reported by Gorbunova (Scheme S1) and Mallory (Scheme S2) [5,6,10–13]. Three routes for the activation of electroless nickel plating are proposed based on the two mechanisms and the work of Hwang and Lin as shown in Fig. 1 (a description in detail can be found in the supporting materials) [7,13–15]. Three routes for the generation of new nuclei for the continuous deposition are as follows: (i) the nuclei are separated from the Ag metal and diffuse into the plating solution, and then are adsorbed/deposited by supports (Fig. 1a); (ii) the nickel ions preadsorbed by supports are reduced by the generating electrons or H atoms (Figs. 1b and 1c); and (iii) the nickel ions near the supports are reduced by the generating electrons or H atoms and adsorbed by the supports (Figs. 1b and 1c). These routes are related to the interface reaction/interaction between the support and the plating solution or the active metal and the plating solution. Little work on the relation has been reported, although the dis-

* Corresponding author. Fax: +86 22 2350 7730.
E-mail address: zhangmh@nankai.edu.cn (M. Zhang).

0021-9797/$ – see front matter
doi:10.1016/j.jcis.2008.10.083

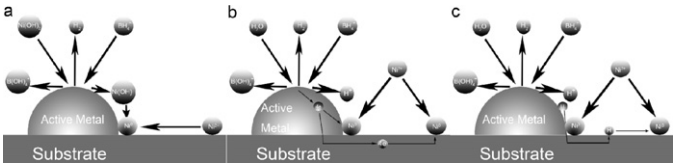

Fig. 1. Processes of nickel deposition on substrates based on (a) hydrolyzed nickel mechanism, (b) electrochemical mechanism, and (c) hydrogen atom mechanism.

persion and size of nickel nanoparticles are mainly affected by the generation of new nuclei [16].

In this paper, the interface reaction/interaction between the support and the plating solution or the active metal and the plating solution in the electroless nickel plating was studied. The mechanism of electroless plating was first studied to point out the factors affecting the dispersion and size of nickel nanoparticles on metal oxides. The changes of the acidity and area of supports and the microwave or ultrasonic wave technique were used to promote the dispersion of nickel nanoparticles. The as-prepared supported nickel nanoparticles were also evaluated in the catalytic hydrogenation of sulfolene and hydrodechlorination of chlorobenzene (see Supporting materials).

2. Materials and methods

2.1. Materials

Nickel(II) sulfate hexahydrate ($NiSO_4{\cdot}6H_2O$), potassium borohydride (KBH_4), ethylenediamine (en) ($H_2NCH_2CH_2NH_2$), sodium hydroxide (NaOH), silver nitrite ($AgNO_3$), 25 wt% ammonia ($NH_3{\cdot}H_2O$), formaldehyde (HCHO), and various metal oxide supports, such as TiO_2, MgO, Fe_3O_4, SiO_2, γ-Al_2O_3, and ZrO_2, were of reagent grade. Doubly distilled water was used in all the experiments.

2.2. Preparation of supported nickel nanoparticles

The Ag/support was synthesized per Refs. [16,17]. From 1.0 to 6.3 g support was added to 425-ml solutions with stirring at 313 K for 4 h. The solution was composed of 4.71×10^{-2} g/L $AgNO_3$, 8.82×10^{-2} g/L ammonia, 1.18×10^{-2} g/L NaOH, and 4.71×10^{-3} g/L HCHO. The resulting Ag/support was collected and washed with distilled water, and then dried at 363 K for 4 h. The electroless nickel plating was performed by adding the Ag/support to the plating solution with the following composition: $NiSO_4{\cdot}6H_2O$, 12.0 g/L; KBH_4, 5.5 g/L; en, 10 g/L; and NaOH, the amount needed to reach pH 13.5. No reactant was added to hold the pH and the concentrations of Ni^{2+} ions and borohydride constant during the plating, and the pH and the concentration of Ni^{2+} decreased with plating time. The reaction lasted until no significant bubbles were observed (about 20–40 min). The product was collected and washed thoroughly with distilled water, and then washed and stored with ethanol. The plating was carried out under conventional heating (water bath) or microwave irradiation (60 W, 2455 MHz) at 323 K. The theoretical nickel loading was controlled between 15 and 20 wt%. The solvents of the plating solution were water and ethylene glycol (EG). An ultrasonic wave (80 W, 40 kHz) was also introduced in some electroless plating experiments. The metal oxides TiO_2, MgO, γ-Al_2O_3, Fe_3O_4, SiO_2, and ZrO_2 were of 200 mesh.

2.3. Instrumentation

The chemical compositions of samples were analyzed by inductively coupled plasma atomic emission spectrometry (ICP-AES) on an IRIS Intrepid spectrometer. Transmission electron microscope (TEM) images were acquired using a JEOL-2010 FEF high-resolution transmission electron microscope equipped with an EDX system (EDAX) and a Philips EM400ST transmission electron microscope. Scanning electron microscope (SEM) images were obtained on a LEO 1530VP field emission instrument. The surface area of the sample was measured using the BET method by N_2 physisorption at 373 K on an automatic surface area and pore size analyzer (Autosorb-1-MP 1530 VP). The UV–vis spectra were recorded on a Cary-100 spectrometer (Varian) equipped with an integration sphere. Barium sulfate was used as a reference. The spectra of solutions were recorded in the range 200–800 nm. The isoelectric point (IEP) was measured as in Ref. [1]. The active nickel surface area (S_{Ni}) of sample was determined by hydrogen chemisorption using a dynamic pulse method [18].

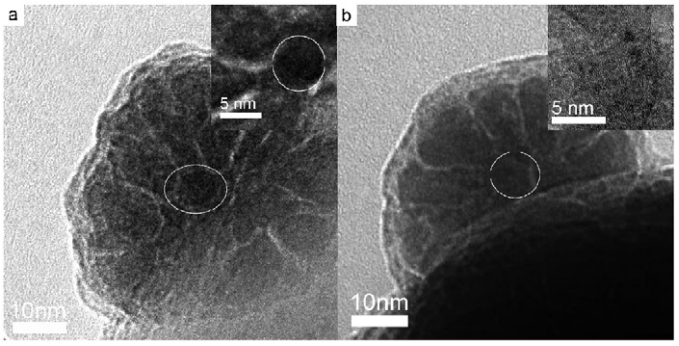

Fig. 2. HRTEM images of nickel nanoparticles in Ni/TiO_2 with 0.16 wt% Ag loading.

3. Results and discussion

3.1. The processes of new nucleus generation and nickel deposition

Electroless metal plating is frequently rethought to proceed by an electrochemical mechanism such as simultaneous of cathodic metal deposition and anodic oxidation of reductant [7,10,15]. The electrochemical conditions for carrying out electroless plating are as follows: The oxidation potential of the reductant is less noble to the reversible potential of the metal to be deposited and the active metal has enough catalytic activity for the anodic oxidation to take place at a reasonable rate [15]. The activation of the plating means that the active metal preloaded on the support catalyzes the anodic oxidation of reductants and induces a potential shift negative to the reversible potential of the metal to be deposited [7,15]. The anodic oxidation of the reductants proceeds mainly by the hydrogen evolution mechanism on copper, silver, and gold and the hydrogen ionization mechanism on cobalt, nickel, palladium, and platinum [15]. The nature and distribution of new active nuclei/species formed during the activation process by the active metal greatly affect the deposition behavior and the properties of the deposit [16].

In our previous work, the nickel nanoparticles were found to be deposited selectively on the TiO_2 or MgO support, rather than formed as a continuous film [17–19]. Fig. 2 shows the HRTEM images of two typical nickel nanoparticles in the Ni/TiO_2 sample with 0.16 wt% Ag loading. One has a dark ellipse in the center of the particle, which is highlighted with a white circle in the insert of Fig. 2a. Its EDX result in Fig. S2a indicates that some Ag elements are observed in the nickel nanoparticle. Because Ag atoms exhibit much higher atomic weight than Ni atoms and the nickel nanoparticle shows an amorphous structure [16–18], the Ag core can be distinguished obviously in the TEM image [18]. This means that the dark ellipse is ascribed to the Ag nuclei. It shows that this type of nickel nanoparticles are formed by the continuous deposition of nickel on the active Ag metal. During the TEM characteriza-

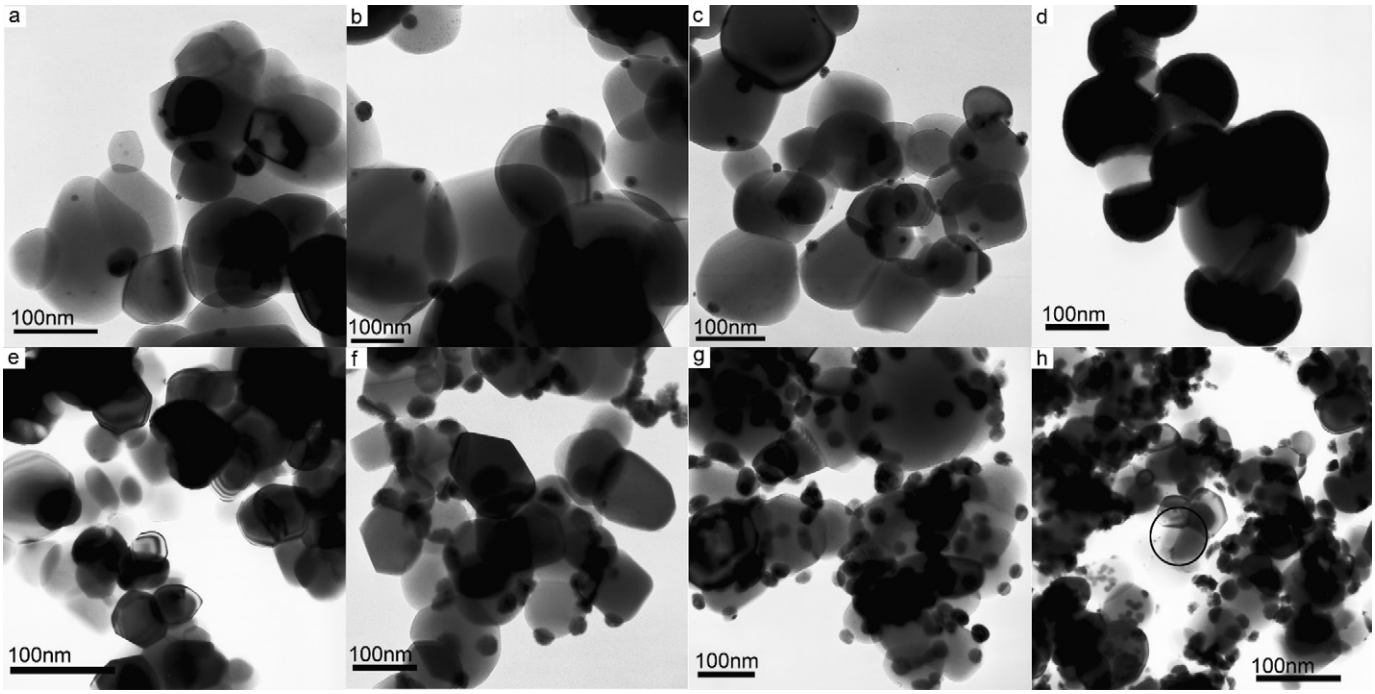

Fig. 3. TEM images of samples with different Ag weight loadings. Ag/TiO_2: (a) 0.02%, (b) 0.05%, and (c) 0.16%. Ni/TiO_2: (d) 0.02%, (e) 0.02%, (f) 0.05%, (g) 0.1%, and (h) 0.16%.

tion, the nickel nanoparticle with a dark backdrop is randomly observed, but a different kind of particles without dark cores are widely found in Fig. 2b. This type of nickel nanoparticle shows a flowlike shape, and the Ag element cannot be detected by EDX characterization (Fig. S2b). This shows that most nickel nanoparticles are formed by the deposition of nickel clusters on the new generating nickel nuclei [16]. Fig. 1 shows two reaction routes for the formation of nickel nuclei. First, the diffusion of nickel colloidal particles from the plating solution during the electroless Ni–P plating on the glass substrates has been reported by Yin et al. and other researchers [20–24]. As shown in Fig. 1a, the dissociative nickel colloidal particles could be formed by separation from the silver surface or by reduction of nickel ions with BH_4^- in the plating solution. The new nuclei are formed by the adsorption or deposition of nickel colloidal particles. It can be concluded that many free nickel nanoparticles without support can be widely observed. Second, the new nuclei are obtained by the reduction of nickel ions adsorbed on or near supports with the electrons or H atoms (Figs. 1b and 1c) generated by the electrochemical or hydrolytic reaction of BH_4^- (Schemes S1 and S2). This means that the new nuclei should mostly be located in the neighborhood of the original silver nuclei or between two original silver nuclei [3,9].

Fig. 3 shows the TEM images of Ag/TiO_2 samples and their resulting Ni/TiO_2 samples. The Ag nanoparticles with diameter 5–10 nm are distributed randomly on TiO_2 as shown. The nickel nanoparticles supported on the Ag/TiO_2 with 0.02 wt% Ag loading show particle size ∼100 nm (Figs. 3a and 3d). With the Ag loading increased from 0.02 to 0.05 wt%, the particle size decreases from ∼100 to ∼40 nm (Figs. 3b and 3f) and the Ni loading increases from 4.5 to 8.1 wt%. It indicates that more new nuclei for the deposition of nickel are formed by promoting the Ag loading. Fig. 1a shows that the dispersion of nickel nuclei on TiO_2 is determined by the diffusion of nickel colloids in the plating solution and the capability of the support to adsorb the nickel colloids. The nucleation sites for the adsorption of nickel colloids are related to the surface defects of supports, such as excess vacancies, dislocations, and grain boundaries [25]. Suitable nucleation sites are nonequilibrium defects that increase the surface free energy of supports. If the creation of a nucleus results in the destruction of a defect, the free energy will be released, thereby reducing the activation energy barrier for nucleation, and the energy of the nullified boundaries helps the nucleation process [25,26]. For the grain boundary triple point, the extent of the grain boundary area nullified during nucleation is larger than that of the boundaries between two grains, and the activation energies for the nucleation are reduced. The nickel colloids on the grain boundaries should be preferentially adsorbed and grow to nuclei because of the lowered activation energy barrier for nucleation. This means that the formation of nickel nuclei for the deposition of nickel is determined by the surface defects of supports. The dispersion of nickel nuclei should be identical for all the Ag/TiO_2 samples and the same size and loading of nickel nanoparticles could be observed on their resulting Ni/TiO_2 samples. But this cannot be confirmed by Fig. 3. A typical TEM image of the Ni/TiO_2 sample with 0.02 wt% Ag loading is shown in Fig. 3e. The nickel nanoparticles are more difficult to observe than those on other Ag/TiO_2 samples with higher Ag loadings. Obviously, the dispersion and size of nickel nanoparticles change with the Ag loading. On the other hand, the nickel nanoparticles are mostly deposited on single TiO_2 grain boundaries, rather than the grain boundary triple point or between two grains. as shown in Figs. 3d–3h (circle in Fig. 3h) and S3 (TEM images of the Ni/TiO_2 sample in different scales). These results indicate that the new nuclei are hardly generated by the adsorption of nickel colloids.

Yin has reported the formation of nickel colloids in the plating solution [20,21]. To study the formation of new nuclei, an experiment on electroless nickel-plating on Ag/Al_2O_3 bars was carried out. One-half of the Al_2O_3 bar was immersed in a 0.1 mol/L $AgNO_3$ solution for 10 min (shown in white), dried in air (shown in yellow), and reduced by 5 ml 0.1 mol/L KBH_4 solution by dropwise addition (shown in gray) in sequence. The as-prepared Ag/Al_2O_3 bar was added to a 100-ml plating solution under stirring as shown in Fig. 4a. The half of the bar loaded with Ag changed from gray to black (Fig. 4b). The bar was transferred to a new 100-ml plating solution after the first plating. Fig. 4c shows that the half of the bar without Ag loading is still presented in white and some new black powder bar is formed. The black powder comes from the separation of nickel nanoparticles from the sup-

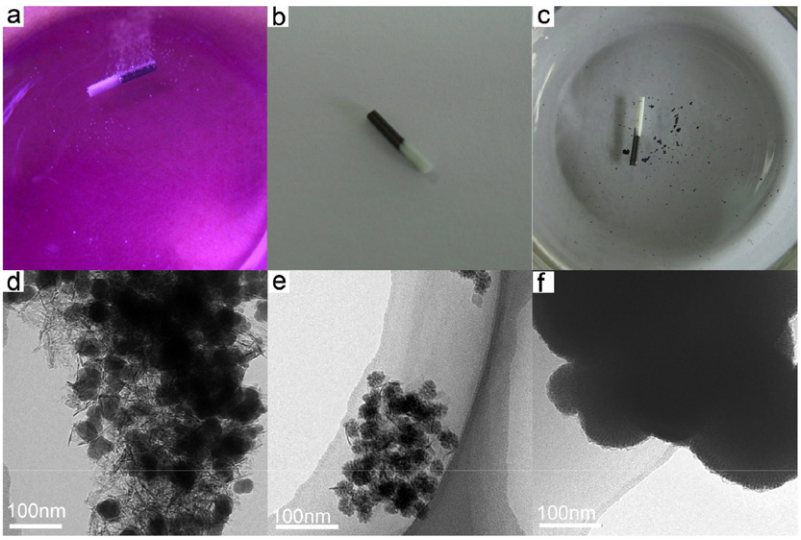

Fig. 4. The phenomenon of plating on the Ag/Al_2O_3 bar and TEM images of its products. (a) Photo of the plating; (b) photo of the Ni/Al_2O_3 bar; (c) photo of the plating product; (d) TEM image of the half of the bar with Ag loading; (e) TEM image of the separated product in (c); and (f) TEM image of the nickel nanoparticles prepared by adding some 1 mol/L $AgNO_3$ containing the same amount of Ag with 0.24 wt% Ag/supports (1.6 g) to the plating solution.

port or the aggregation of nickel colloids in the plating solution. The TEM characterization shows that such powder exhibits a particle size (15–20 nm in Fig. 4e) much smaller than that (30–35 nm in Fig. 4d) of supported nickel nanoparticles. Few nickel nanoparticles are observed on the half without Ag loading from the TEM characterization. This shows that the nickel colloids are hardly adsorbed or deposited on the Al_2O_3 support, and the new powder is formed by the aggregation of nickel colloids. Therefore, the formation of new nuclei is not mainly determined by the adsorption of nickel colloids in the plating solution. The result is also agreed upon by Boonekamp et al. [27].

Table S1 shows that the plating time decreases and the Ni loading increases with the Ag loading on supports. The number of active Ag sites increases with Ag loading, which shortens the activation time (the time for the formation of new nuclei) for plating and thus the plating time. Fig. 2b shows that most nickel nanoparticles are formed by the continuous deposition of nickel on the new nickel nuclei. Figs. 1b and 1c show that the new nuclei occur in two routes: The nickel ions preadsorbed by supports are reduced by the generating electrons or H atoms, and the nickel ions adjacent to the surfaces of supports are reduced by the generating electrons or H atoms and adsorbed by supports. It is obvious that the number of new active nuclei increases with Ag loading. This can explain the difference in the dispersion and size of nickel nanoparticles among the Ni/TiO_2 samples with different Ag loadings. Few new nuclei are generated by the Ag/TiO_2 with 0.02 wt% Ag loading and the resulting nickel nanoparticles grow to ~100 nm. Kelly and Vondeling studied the minimum number of palladium atoms required to initiate/catalyze the electroless nickel plating [28]. Active sites containing at least four palladium atoms can catalyze the electroless nickel deposition [29]. More and larger active metal sites promote catalysis of the anodic oxidation of borohydride and shift the potential to less negative than the reversible potential of the metal to be deposited [30]. The surface number, concentration, and size of Ag sites increase with the growth of Ag loading. This results in two possible paths for creating higher dispersion and smaller size of nickel nanoparticles on TiO_2, as shown in Fig. 3: (i) the density of the active sites for the deposition of nickel increases and limits the room available for lateral growth, and (ii) the catalytic surface where the deposition sites are contained is formed within a narrow distribution shifted to smaller particle sizes [30]. As shown in Figs. 3f–3h, more new nuclei are generated by increasing Ag loadings and provide sufficient sites for the deposition to reduce the size to ~40 nm. A higher density of new active sites can also promote the coalescence of neighboring particles to form a continuous film (Fig. S4, TEM images of Ag/TiO_2 with 5 wt% Ag loading and its corresponding Ni/TiO_2 sample). The results show that the load and size of Ag on TiO_2 affect the dispersion and size of nickel nanoparticles. In addition, the size of nickel nanoparticles has been proved to be decreased by promoting the dispersion of the Ag particles [31]. Here, the dispersion of nickel nanoparticles increases and the size decreases by increasing Ag loadings.

Although the new nuclei are not mainly generated by the adsorption of nickel colloids, it is still difficult to distinguish the electrochemical mechanism (Scheme S1) and the hydrolyzed nickel mechanism (Scheme S2) here. The TiO_2 has been regarded as the electronic conductive material [32–34], and the electrochemical mechanism is possible from various characterizations. On the other hand, the hydrogen spillover phenomenon was found on TiO_2 loaded with metals in the 1960s [35]. The hydrogen spillover through silver on Ag/TiO_2 has been proved by Wang and Yeh [36]. The borohydride is anodically oxidized on the surface of the Ag metal accompanied by an evolution of hydrogen atoms and gas in the electroless plating [15,23]. This allows the nickel ions absorbed around the Ag sites to be reduced by the resulting hydrogen atoms. The main difference in the formation of new nuclei between Schemes S1 and S2 is ascribed to the reductant used for nickel ions: electrons in Scheme S1 and H atoms in Scheme S2. Thus, the surface concentration and the dispersion of new nuclei should be dependent on the interface reaction between supports and the nickel ions: (i) the nickel ions are adsorbed by the supports and reduced by the generating electrons or H atoms, and (ii) the nickel ions adjacent to the surfaces of supports are reduced by the generating electrons or H atoms and adsorbed or deposited by the supports. In short, the promotion of the dispersion of nickel nanoparticles is attributed to increasing concentrations of nickel ions absorbed or around the surfaces of supports. The simplest method is to increase the concentration of the nickel ions. But a higher concentration leads to worse stability and shorter lifetimes for the plating solution [8,9]. More attempts should be focused on the study of the interfacial deposition of nickel ions on oxide carriers [4,5].

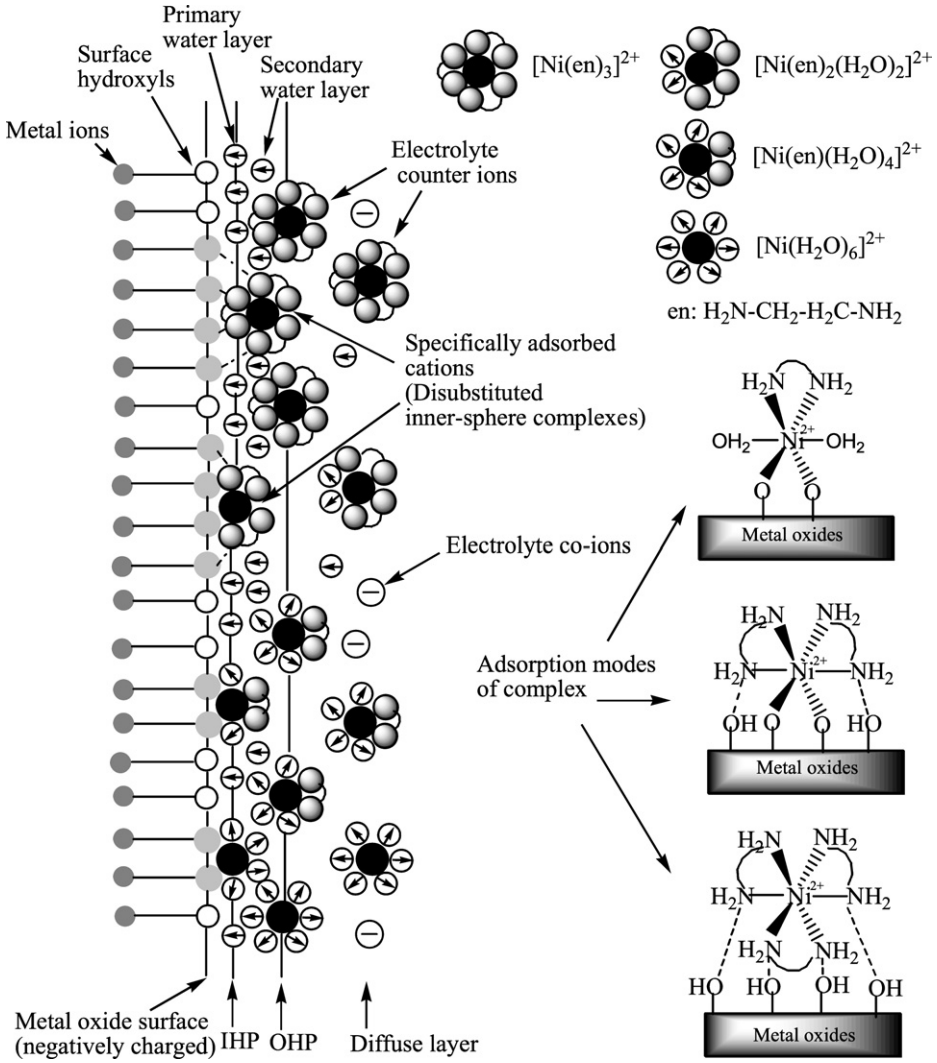

Fig. 5. A schematic illustration of the electrical double layer between the surface of metal oxides and the plating solution and the adsorption modes of nickel complexes. By IHP we symbolize the so-called inner Helmholtz plane, and by OHP the so-called outer Helmholtz plane. For simplicity we use the term "surface hydroxyls" to describe unprotonated or singly or doubly protonated surface oxygen, and we consider only singly coordinated surface oxygen.

3.2. The effects of the surface properties of supports on electroless nickel plating

Bourikas et al. summarized various modes of the interfacial deposition of transition metal ions on an oxide carrier [4; see also 5]. Many more cases reported in the literature concern specific adsorption related to the formation of surface inner-sphere complexes. Yin et al. proposed a mode of the electric double layer likely to be formed in electroless Ni–P plating [20–23]. Che et al. studied the role of the surface of metal oxides on the coordination chemistry of transition metal ions [37–43]. The structure of the interfacial surface between the metal oxide and the plating solution is illustrated (Fig. 5) based on the work above. Transition metal complexes (TMCs) with various stoichiometries coexist in solutions. For example, TMCs in aqueous solution contain six aqua ligands. As the bidentate ligand, en is added to the solution, TMCs undergo several successive reactions of complexation through which chelating ligands replace H_2O molecules [42,43]. The new complexes are more stable because the chelating ligands remain bonded to metal ions, while the labile monodentate H_2O ligands are replaced by the surface groups of the metal oxide upon grafting. TMCs with different numbers of chelating ligands thus exhibit different reactivities toward the surface of metal oxides.

Fig. 5 shows that nickel ions are coordinated by H_2O or en in the plating solution. The interactions between cations, ligands or counterions, and the surfaces of metal oxides occur at the initial stage of plating. The occurrence plays a crucial role in the dispersion of new active nuclei. Strong metal–support interactions generally favor a uniform distribution of new active sites [42]. Che and co-workers pointed out three types of adsorption modes of nickel complexes with different en contents, as shown in Fig. 5 [37–44]. UV–vis spectroscopy is used to confirm the structure of nickel complexes in the aqueous solution of nickel ions and en (Fig. 6a) and the plating solution (Fig. 6b). Two broad bands around 340 and 550–600 nm are observed in the aqueous solution with different en/Ni molar ratios. These bands are assigned to the spin-allowed d–d transitions $3A_{2g} \rightarrow 3T_{1g}$ (F) (λ_1) and $3A_{2g} \rightarrow 3T_{1g}$ (P) (λ_2) of octahedral Ni^{2+} (d^8) [42,44]. A blue shift is found by increasing the en/Ni molar ratio because the bonding between en and nickel ions becomes stronger with increasing en/Ni ratio. The aqueous solution with en/Ni ratio at 4 shows two peaks at 350 and 550 nm in Fig. 6a. The corresponding complex $[Ni(en)_x(H_2O)_{(6-2x)}]^{2+}$ should be $[Ni(en)_3]^{2+}$ mostly, concomitant with some $[Ni(en)_2(H_2O)_2]^{2+}$ [42,45]. The same peaks are also observed in the plating solution from Fig. 6b, suggesting that the structure of $[Ni(en)_x(H_2O)_{(6-2x)}]^{2+}$ changes little with the addi-

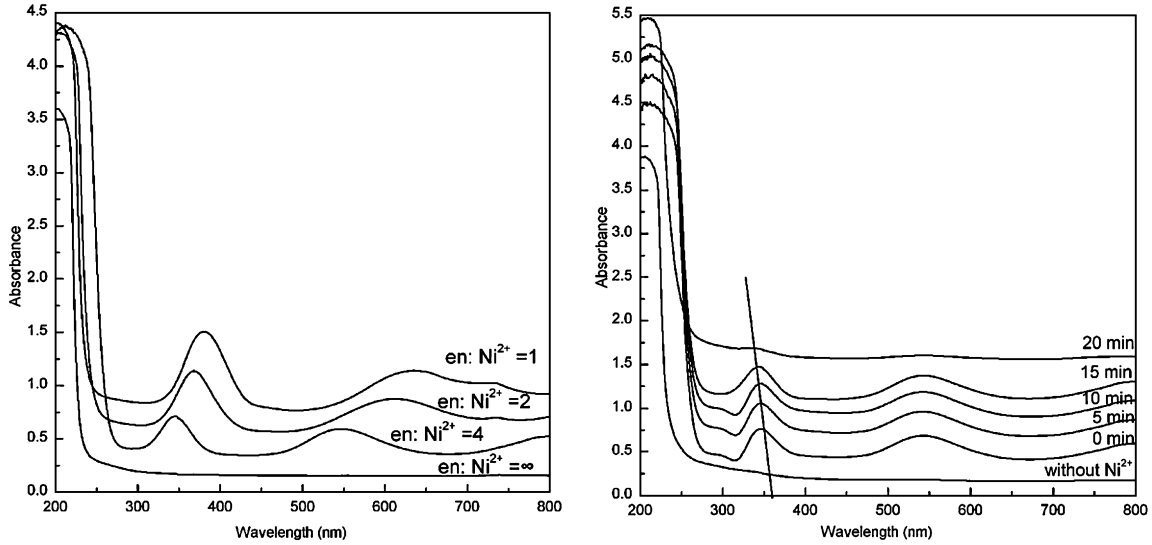

Fig. 6. (a) UV–vis spectra of $[Ni(en)_x(H_2O)_{(6-2x)}]^{2+}$ in the aqueous solutions prepared with different nominal en/Ni^{2+} ratios; and (b) UV–vis spectra of $[Ni(en)_x(H_2O)_{(6-2x)}]^{2+}$ in the plating solution prepared with nominal en/Ni^{2+} ratio of 4 at different plating times.

tion of borohydride and NaOH. The strong interaction between the en ligands bonded to nickel ions and metal oxides mainly occurs between the –NH groups and the surface hydroxyls of metal oxides, as shown in Fig. 5. Fig. 6b shows the UV–vis spectra of nickel complexes during the electroless nickel plating on TiO_2 support. After the addition of Ag/TiO_2 with 1.1 wt% Ag loading to the plating solution, a decrease of pH from 13.5 to 13.2 within 12 min of plating is observed. This could be explained by the receptor sites or neighbor surface groups being deprotonated upon adsorption through coordination of nickel ions having positive charges in order to compensate for the positive charges transferred to the surface [4,5,42]. Therefore, the decrease of pH indicates the formation of inner sphere complexes by the nickel ions, en, and the surface of supports (Fig. 5) [46–48]. In our previous work [14,15], the activation time was found to be ∼12 min. A blue shift is observed by increasing the plating time (Fig. 6b), suggesting that the content of $[Ni(en)_3]^{2+}$ increases and the nickel complexes are deposited or adsorbed by the support gradually. The preadsorbed nickel complex also acts as the reception site, which promotes the adsorption of the nickel complexes. This causes the formation of multinuclear nickel complexes and thus the surface precipitates of nickel ions [4,5,49]. Thus more new nuclei with required particle size [28,29] are generated by the reduction of the multinuclear nickel complexes by electron or hydrogen atoms on the surfaces of metal oxides. Fig. 6b shows that the concentration of nickel ions changes little during the first 15 min of plating, but the new active sites are widely observed by the TEM characterization [16]. The results show that the new nuclei are formed by reducing the inner sphere complexes with electrons or hydrogen atoms. It has been reported that the inner sphere complexes lead to higher dispersion and stronger “support–supported phase” interaction on the supported metal nanoparticles prepared by the impregnation method than on those prepared by “electrostatic/hydrogen bonding” interfacial deposition [4,5]. Tables 1 and S2 show the changes of activation time, plating time, nickel loading, and pH during plating. Different decreases have been observed when different metal oxides are used (Table S2). For example, a greater decrease (0.6) occurs on MgO than on TiO_2 (0.3) at the beginning of electroless plating. This means that the interaction/interface reaction of –NH groups in nickel complexes and the surface groups of MgO becomes more intense than that on TiO_2, suggesting that the surface sites for the adsorption of nickel complexes increase on MgO and more new active nuclei for nickel deposition are formed. Thus, the nickel loading and plating rate increase from ∼10 wt% on TiO_2 to ∼15 wt% MgO (Tables 1 and S2), while the size of nickel particles is similar at ∼40 nm (Figs. S5 and S10). In short, the dispersion of the new active sites is determined by the interface reaction between the surface of supports and the nickel complexes.

The TEM images of the Ag/supports, such as Ag/MgO, Ag/γ-Al_2O_3, Ag/Fe_3O_4, Ag/ZrO_2, and Ag/SiO_2, and the resulting Ni/supports are shown in Figs. S5–S9. The pH of the plating solution decreases below 13.3 immediately after the addition of Ag/supports with 0.24 wt% Ag loading, as shown in Table S2. When some 1 mol/L $AgNO_3$ containing the same amount of Ag was added to the plating solution, the pH changed from 13.5 to 13.3 until no bubbles were observed. The γ-Al_2O_3 can dissolve in a strong basic solution [50], and the one with greater surface area dissolves much more. This leads to a lower pH of 12.9 and a lower nickel deposition rate (Tables 1 and S2) [8,9]. Tables 1 and S2 show that more decrease of pH and less activation time and plating time are observed on the metal oxide with higher IEP. Boujday et al. [51–53] and others [4,5] have studied the adsorption of the nickel complexes, $[Ni(en)_2(H_2O)_2]^{2+}$, at the amorphous silica/electrolyte solution interface. The EXAFS found that hydrogen bonds are formed between the –NH groups of the en and the neighboring silanol/silanolate groups or oxygen atoms of the ···Si–O–Si··· siloxane linkages participating in the constrained rings of three or four SiO_4 tetrahedra. These rings impose special geometries of the ···Si–O–Si··· linkages, which increase the reactivity of the siloxane oxygen atoms. Thus, the low surface concentration of the adsorbed nickel complexes as compared to the silanol concentration is ascribed to the low concentration of the constrained rings. This means that the surface concentration of the adsorbed nickel complexes varies with different metal oxides, as the kind of groups (surface density and the excess charge of oxygen) exposed on the surface of each metal oxide is different. Table 1 presents the nickel loading on the different metal oxides prepared by the electroless plating and the impregnation method. Except for γ-Al_2O_3, with much higher surface area, the nickel loading is promoted by increasing the IEP of metal oxides. This shows that the capability of metal oxides to adsorb nickel complexes increases with the IEP of metal oxide support. A higher plating rate and nickel loading are observed on the basic metal oxides (Table 1). The particle sizes of nickel on MgO, Fe_3O_4, and SiO_2 with similar surface ar-

Table 1
The properties of supports and their effects on electroless nickel plating and Ni loading on supports.

Samples	Isoelectric point (IEP)	S_{BET} (m^2/g)	Activation time (min)[a]	Plating time (min)	Ni loading (wt%)[b]		
					A	B	C
MgO	12.1	4	7	18	3.1	2.8	15.1
γ-Al_2O_3(s)	8.2	117	10	25	3.9	3.1	14.4
γ-Al_2O_3(l)	8.1	456	11	24	4.3	3.7	14.6
ZrO_2	6.1	102	9	30	1.8	1.4	11.1
Fe_3O_4	5.4	2	11	30	1.6	1	10.8
TiO_2	4.8	18	12	32	1.6	1.1	10.8
SiO_2	2.2	4	24	38	0.5	0.1	9.2

[a] Activation time: the time for fully generating new active nuclei for nickel deposition. It is generally the same as the time from adding Ag/support to generation of bubbles, as shown in Ref. [16].

[b] The Ni loading on Ag/supports from (A) 5 min electroless plating; (B) 5 min impregnation of Ag/supports in the plating solution without KBH_4; (C) the whole plating on Ag/support with 0.24 wt% Ag loading.

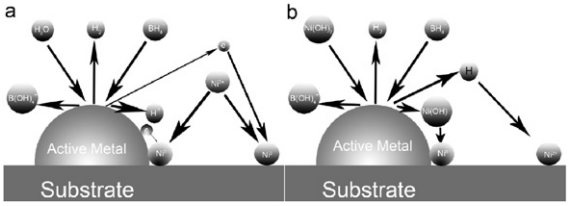

Fig. 7. Processes of nickel deposition on substrates based on (a) the electrochemical mechanism and (b) the hydrolyzed nickel mechanism.

eas are varied from ~40 to 300 nm (Figs. S5–S9). These indicate that the basic metal oxide is a better choice for the adsorption of nickel complexes. The surface area also affects the adsorption of nickel complexes. For example, the γ-Al_2O_3(l) with higher surface area could adsorb more nickel complexes, and more active sites for deposition are formed to prepare dispersed nickel nanoparticles (Fig. 5). On the other hand, the adsorption of nickel complexes is also affected by the pH based on the adsorption mode proposed in Fig. 5. Bourikas et al. pointed out that the modes of the adsorption of transition metal ions were greatly varied with the pH and the metal concentrations [4,5]. For the electroless plating, the structure of complexes and pH are changed with the concentration of nickel and BH_4^- ions [8,9]. The concentration of $[Ni(en)_3]^{2+}$ increases while that of the $[Ni(en)_2(H_2O)_2]^{2+}$ decreases, which means that the interface reaction of the surface of supports and the –NH groups is strengthened [42,45]. This shows that the formation of new active sites is mainly affected by the interface reaction between –NH groups and the surfaces of metal oxides. Therefore, the acidity and surface area of metal oxides should be carefully selected, as the composition of the plating solution is usually confirmed. Thus, the metal oxide with higher IEP and surface area is favored by high dispersion of nickel nanoparticles.

In this section, the dispersion of nickel nanoparticles is found to be dependent on the adsorption capability of nickel complexes by metal oxides. The SiO_2, Al_2O_3, ZrO_2, and MgO are electronic nonconductive supports, and their hydrogen spillover phenomena have been little reported. New modes of formation of new nickel nuclei by reducing the absorbed nickel ions with electrons or H atoms are proposed in Fig. 7. Fig. 7a shows that the silver metals are the catalytically active anode where the oxidation of borohydride occurs to produce electrons; the sites at the cathodes around the silver anodes adsorbed the nickel complexes with the addition of supports to plating solution, and the new active nuclei are formed by reducing these nickel complexes with their neighboring electrons. The reductant is changed from the electron to the hydrogen atom generated by the decomposition of borohydrides, as shown in Fig. 7b. The occurrence of new active nuclei in Fig. 7 is the same as in Figs. 1b and 1c. These modes can be supported by the work of Yin et al. [20–22], as the nickel colloids are generated by reducing nickel ions with electrons and hydrogen atoms diffused in the plating solution. But it is still difficult to point out a mechanism for the electroless plating. The conclusion that the dispersion and size of nickel on metal oxides are determined by the adsorption capability of nickel complexes can be confirmed.

3.3. Synthesis of supported nickel nanoparticles by introducing microwaves and ultrasound waves

Section 3.2 shows that the adsorption/deposition of nickel ions by supports is the result of the competitive sorption between en (–NH groups) and H_2O. Conner and co-workers studied the effect of microwave irradiation on the sorption of metal oxides [54–58]. The adsorbates with different dielectric constants (ε, 293 K) exhibit different capabilities to adsorb microwave energy, and the adsorbates are adsorbed/deposited selectively on metal oxides under microwave irradiation [17]. The ε of H_2O (58.8) is higher than that of en (8.85) [59,60]. The interface reaction between H_2O and the surfaces of metal oxides is strengthened by the microwave energy [54–58]. The interface reaction between the en and the surface of TiO_2 is weakened, and the number of adsorption sites for nickel complexes decreases, which reduces the new active sites for nickel deposition. This makes the size of nickel nanoparticles (~60 nm) on Ni/TiO_2 prepared under microwave irradiation larger than that (~40 nm) with conventional heating, as shown in Fig. S10. Fig. S11 (TEM images of Ni/MgO with ~15 wt% Ni loading prepared under conventional heating and microwave irradiation) shows the same growth of particle size after microwave irradiation. A decrease of the number of new active sites is obviously observed in the corresponding SEM images, as shown in Fig. S12 (SEM images of Ni/MgO with ~15 wt% Ni loading synthesized by conventional heating and microwave irradiation). Fig. S13 shows the TEM images of Ni/MgO with ~11 wt% Ni loading prepared in an ethylene glycol bath with heating by conventional heating and microwave irradiation. The size of nickel nanoparticles changes less, from ~40 to ~45 nm, as ethylene glycol shows a smaller ε (26.33) than H_2O.

The effects of ultrasonic irradiation on electroless nickel plating have already been studied by many researchers [61,62]. It has been concluded that the plating rate is increased by introducing ultrasound waves. Touyeras et al. studied the effect of ultrasonic irradiation on electroless copper plating with Pd as the active metal [63]. Pd plays a major role in generating more new active copper nuclei under ultrasonic irradiation. Fig. S14 shows the TEM images of Ni/TiO_2 prepared under ultrasonic irradiation for different times. The nickel loadings are ~10 wt%, but the size of nickel nanoparticles decreases from 40 to 10 nm with prolongation of the irradiation time from 0 to 20 min. This suggests that the density of nickel nanoparticles on TiO_2 increases with ultrasonic irradiation, which indicates that the dispersion of nickel nanoparticles is promoted. Table S3 and Fig. S15 show that the control of the dispersion and size of nickel nanoparticles promote catalytic activity and stability in the hydrogenation of sulfolene and the hydrodechlorination of chlorobenzene.

4. Summary

Nickel nanoparticles supported on metal oxides were prepared by a modified electroless plating method. Generation processes for new nickel nuclei for the deposition of nickel were proposed to summarize the reported plating mechanisms. The study was focused on the discussion of the processes based on the experimental and characterization results, in order to clarify the mechanism for electroless nickel-plating on metal oxides. For example, the activation process was investigated by changing the Ag loading (the

dispersion and load of silver metals) and the properties of supports (the surface acidity and area). A schematic illustration of the electrical double layer between the surface of metal oxides and the plating solution and the modes of adsorption of nickel complexes by the surface of metal oxides was proposed. The TEM characterizations showed that the dispersion of nickel nanoparticles was promoted by increasing Ag loading, as more new active nickel nuclei for deposition occurred. The BET and IEP characterizations indicated that the IEP and surface area of metal oxides affected the generation of new active nickel nuclei, and the dispersion of nickel nanoparticles was improved by increasing the IEP and surface area. Meanwhile, the dispersion or size of nickel nanoparticles could also be changed by introducing microwave and ultrasonic irradiation to affect the adsorption of nickel complexes onto metal oxides. The results showed that the electroless plating was the result of interface reactions/interactions between the surface of the supports and the plating solution, and the number and dispersion of new active nickel nuclei were dependent on the interface reactions: the nickel complexes preadsorbed by supports were reduced by the generating electrons or hydrogen atoms; and the nickel complexes adjacent to the supports were reduced by generation electrons or hydrogen atoms and were deposited on supports. The electroless plating method was an effective route to synthesize supported nickel nanoparticles with controlled variable dispersions and sizes. In a word, the work on what controlled the dispersion and size of nickel nanoparticles during plating, and how, was carried out, and the knowledge and experience were revealed to be helpful and important for the preparation of other supported metal (Fe, Co, or Cu) nanoparticles.

Acknowledgments

This work was supported by the NSF of China (20403009) and a Key Project of the Chinese Ministry of Education (105045).

Supporting materials

The online version of this article contains additional supporting materials.

Please visit DOI: 10.1016/j.jcis.2008.10.083.

References

[1] G.A. Parks, Chem. Rev. 65 (1965) 177.
[2] J.P. Brunelle, Pure Appl. Chem. 50 (1978) 1211.
[3] S. Subramanian, J.S. Noh, J.A. Schwarz, J. Catal. 114 (2) (1988) 433.
[4] K. Bourikas, C. Kordulis, A. Lycourghiatis, Catal. Rev. Sci. Eng. 48 (2006) 363.
[5] J. Hagen, Industrial Catalysis. A Practical Approach, Wiley–VCH, New York, 2006, chap. 2.
[6] Z.J. Wu, W. Li, M.H. Zhang, K.Y. Tao, Front. Chem. Eng. China 1 (2007) 87.
[7] B.J. Hwang, S.H. Lin, J. Electrochem. Soc. 142 (1995) 3749.
[8] G.O. Mallory, J.B. Hajdu, Electroless Plating: Fundamentals and Applications, American Electroplaters and Surface Finishers Society, Orlando, FL, 1990, pp. 1–56.
[9] T.C. Wang, B. Chen, M.R. Rubner, R.E. Cohen, Langmuir 17 (2001) 6610.
[10] K.M. Gorbunova, M.V. Ivanov, V.P. Moiseev, J. Electrochem. Soc. 120 (1973) 613.
[11] G. Mallory, Plating 58 (1971) 319.
[12] P. Cavallotti, G. Salvago, Electrochim. Metall. 3 (1968) 239.
[13] J.P. Marton, M. Schlesinger, J. Electrochem. Soc. 115 (1) (1968) 16.
[14] T. Homma, T. Yamazaki, T. Osaka, J. Electrochem. Soc. 139 (1992) 732.
[15] I. Ohno, O. Wakabayashi, S. Haruyama, J. Electrochem. Soc. 132 (1985) 2323.
[16] Z.J. Wu, M.H. Zhang, S.H. Ge, Z.L. Zhang, W. Li, K.Y. Tao, J. Mater. Chem. 15 (2005) 4928.
[17] S.H. Ge, Z.J. Wu, M.H. Zhang, W. Li, K.Y. Tao, Ind. Eng. Chem. Res. 45 (2006) 2229.
[18] Z.J. Wu, S.H. Ge, M.H. Zhang, W. Li, S.C. Mu, K.Y. Tao, J. Phys. Chem. C 111 (2007) 8587.
[19] Z.J. Wu, M.H. Zhang, W. Li, S.C. Mu, K.Y. Tao, J. Mol. Catal. A 273 (2007) 277.
[20] X. Yin, L. Hong, B.H. Chen, T.M. Ko, J. Colloid Interface Sci. 262 (2003) 89.
[21] X. Yin, L. Hong, B.H. Chen, J. Phys. Chem. B 108 (2004) 10919.
[22] C.H. Chen, B.H. Chen, L. Hong, Chem. Mater. 18 (2006) 2959.
[23] G.A. Walker, C.C. Goldsmith, Thin Solid Films 53 (1978) 217.
[24] J. Shu, B.P.A. Gradjean, E. Ghali, S. Kaliagvine, J. Electrochem. Soc. 140 (1993) 3175.
[25] S.W. Hong, Y.S. Lee, K.C. Park, J.W. Park, J. Electrochem. Soc. 150 (2003) C16.
[26] D.A. Porter, K.E. Easterling, Phase Transformations in Metals and Alloys, Van Nostrand Reinhold, New York, 1981, chap. 5.
[27] F.P. Boonekamp, J.J. Kelly, L.G.J. Fokkink, D.W.E. van den Houdt, J. Electrochem. Soc. 142 (1995) 519.
[28] J.J. Kelly, J.K. Vondeling, J. Electrochem. Soc. 122 (1975) 1103.
[29] J.F. Hamilton, P.C. Logel, J. Catal. 29 (1973) 253.
[30] S.J. Brandow, W.J. Dressick, C.R.K. Marrian, G.M. Chow, J.M. Calvert, J. Electrochem. Soc. 142 (1995) 2233.
[31] M.X. Wu, W. Li, M.H. Zhang, K.Y. Tao, Chinese J. Catal. 28 (2007) 351.
[32] P.K. Kofstad, Nonstoichiometry, Diffusion and Electrical Conductivity in Binary Metal Oxides, Wiley, New York, 1972.
[33] C.N.R. Rao, G.V. Subba Rao, Phys. Status Solidi A 1 (2006) 597.
[34] C.J. Kevane, Phys. Rev. 133 (1964) A1431.
[35] T. Inui, K. Fujimoto, T. Uchijima, M. Masai (Eds.), New Aspects of Spillover Effect in Catalyst, in: Stud. Surf. Sci. Catal., vol. 77, Elsevier, Amsterdam, 1993.
[36] Y.P. Wang, C.T. Yeh, J. Chem. Soc. Faraday Trans. 87 (1991) 345.
[37] M. Che, L. Bonneviot, Pure Appl. Chem. 60 (1988) 1369.
[38] Z. Sojka, M. Che, Chimie 3 (2000) 163.
[39] F. Negrier, É. Marceau, M. Che, D.C.R. Caro, Chimie 6 (2003) 231.
[40] F. Négrier, E. Marceau, M. Che, J.M. Giraudon, L. Gengembre, A. Löfberg, J. Phys. Chem. B 109 (2005) 2836.
[41] O. Clause, M. Kermarec, L. Bonneviot, F. Villain, M. Che, J. Am. Chem. Soc. 114 (1992) 4709.
[42] K.Q. Sun, E. Marceau, M. Che, Phys. Chem. Chem. Phys. 8 (2006) 1731.
[43] X. Carrier, E. Marceau, M. Che, Pure Appl. Chem. 78 (2006) 1039.
[44] L. Bonneviot, O. Legendre, M. Kermarec, D. Olivier, M. Che, J. Colloid Interface Sci. 134 (1990) 534.
[45] P. Paoletti, Pure Appl. Chem. 56 (1984) 491.
[46] G.D. Panagiotou, T. Petsi, J. Stavropoulos, K. Bourikas, C. Kordulis, A. Lycourghiotis, Stud. Surf. Sci. Catal. 162 (2006) 809.
[47] K. Bourikas, G.D. Panagiotou, T. Petsi, C. Kordulis, A. Lycourghiotis, Stud. Surf. Sci. Catal. 162 (2006) 251.
[48] C.J. Chisholm-Brause, P.A. O'Day, G.E. Brown Jr., G.A. Parks, Nature 348 (1990) 528.
[49] K. Bourikas, Ch. Kordulis, J. Vakros, A. Lycourghiotis, Adv. Colloid Interface Sci. 110 (2004) 97.
[50] X. Carrier, E. Marceau, J.F. Lambert, M. Che, J. Colloid Interface Sci. 308 (2007) 429.
[51] S. Boujday, J.F. Lambert, M. Che, Phys. Chem. Phys. Chem. 5 (2004) 1003.
[52] S. Boujday, J. Lehman, J.F. Lambert, M. Che, Catal. Lett. 88 (2003) 23.
[53] S. Boujday, J.F. Lambert, M. Che, J. Phys. Chem. B 107 (2003) 651.
[54] M.D. Turner, R.L. Laurence, K.S. Yngvesson, W.C. Conner, Catal. Lett. 71 (2000) 133.
[55] S.J. Vallee, W.C. Conner, J. Phys. Chem. B 110 (2006) 15459.
[56] C. Reichardt, Solvents and Solvent Effects in Organic Chemistry, VCH, Weinheim, 1988.
[57] M.D. Turner, R.L. Laurence, W.C. Conner, K.S. Yngvesson, AIChE J. 46 (2000) 758.
[58] W.C. Conner, G.A. Tompsett, J. Phys. Chem. B 108 (2004) 13913.
[59] G.A. Tompsett, W.C. Conner, K.S. Yngvesson, Chem. Phys. Chem. 7 (2006) 296.
[60] Z.J. Wu, S.H. Ge, M.H. Zhang, W. Li, K.Y. Tao, Catal. Commun. 9 (2008) 1432.
[61] E.P. Boonekamp, J.J. Kelly, L.G.J. Fokkink, D.W.E. van den Houdt, J. Electrochem. Soc. 142 (1995) 529.
[62] M.Y. Abyaneh, A. Sterritt, T.J. Mason, J. Electrochem. Soc. 154 (2007) D467.
[63] F. Touyeras, J.Y. Hihn, X. Bourgoin, B. Jacques, L. Hallez, V. Branger, Ultrason. Sonochem. 12 (2005) 13.